



Published in final edited form as:

J Nucl Med. 2014 June ; 55(6): 960–966. doi:10.2967/jnumed.113.132928.

PARAMETRIC IMAGING AND TEST-RETEST VARIABILITY OF ^{11}C -(+)-PHNO BINDING TO D_2/D_3 DOPAMINE RECEPTORS IN HUMANS ON THE HRRT PET SCANNER

Jean-Dominique Gallezot¹, Ming-Qiang Zheng¹, Keunpoong Lim¹, Shu-fei Lin¹, David Labaree¹, David Matuskey^{1,2}, Yiyun Huang¹, Yu-Shin Ding^{1,3}, Richard E. Carson¹, and Robert T. Malison²

¹PET Center, Department of Diagnostic Radiology, Yale University School of Medicine, New Haven, CT 06520

²Department of Psychiatry, Yale University School of Medicine, New Haven, CT 06520

³Department of Radiology and Psychiatry, New York University School of Medicine, New York, NY, USA

Abstract

^{11}C -(+)-PHNO is an agonist radioligand for imaging dopamine D_2 and D_3 receptors in the human brain with PET. In this study we evaluated the reproducibility of ^{11}C -(+)-PHNO binding parameters using a within-day design and assessed parametric imaging methods.

Methods—Repeated studies were performed in eight subjects, with simultaneous measurement of the arterial input function and plasma free fraction. Two ^{11}C -(+)-PHNO scans on the same subject were separated by 5.4 ± 0.7 h. After evaluating compartment models, ^{11}C -(+)-PHNO volumes of distribution V_T and V_T/f_p and binding potentials BP_{ND} , BP_P and BP_F were quantified using the multilinear analysis MA1, with the cerebellum as reference region. Parametric images of BP_{ND} were also computed using SRTM and SRTM2.

Results—The test-retest variability of ^{11}C -(+)-PHNO BP_{ND} was 9% in D_2 -rich regions (caudate and putamen). Among D_3 -rich regions, variability was low in pallidum (6%), but higher in substantia nigra (19%), thalamus (14%) and hypothalamus (21%). No significant mass carry-over effect was observed in D_3 -rich regions, although a trend in BP_{ND} was present in substantia nigra ($-14 \pm 15\%$). Due to the relatively fast kinetics, low noise BP_{ND} parametric images were obtained with both SRTM and SRTM2 without spatial smoothing.

Conclusion— ^{11}C -(+)-PHNO can be used to compute low noise parametric images in both D_2 and D_3 rich regions in humans.

Corresponding author: Jean-Dominique Gallezot, Positron Emission Tomography (PET) Center, Yale University, 801 Howard Avenue, PO Box 208048, New Haven, CT 06520-8048. Phone: 1 203 737-9738. Fax: 1 203 785-3107. jean-dominique.gallezot@yale.edu.

Disclaimer: None

Its contents are solely the responsibility of the authors and do not necessarily represent the official view of NIH.

Keywords

Dopamine D2 Receptor; Dopamine D3 Receptor; Agonist; Positron Emission Tomography; Test-Retest Study

INTRODUCTION

^{11}C -(+)-PHNO is a tracer used to study dopamine D_2 and D_3 receptors (D_2R and D_3R) in vivo with positron emission tomography (PET) (1). As an agonist tracer (2), ^{11}C -(+)-PHNO is useful to study the high-affinity states of $\text{D}_2\text{R}/\text{D}_3\text{R}$ and to amplify the signal in studies of dopamine release (3). Other available $\text{D}_2\text{R}/\text{D}_3\text{R}$ agonist radioligands include ^{11}C -NPA and ^{11}C -MNPA. In contrast to existing radioligands, however, ^{11}C -(+)-PHNO is D_3R -preferring with a 30–50 fold higher affinity for D_3R than for D_2R both in vitro (4) and in vivo (5). Therefore, ^{11}C -(+)-PHNO specific binding derives from contributions of both D_2R and D_3R , in proportions that vary across regions based on their respective densities. The D_3R fraction of specific binding ranges from 0% in the putamen to 100% in the substantia nigra (SN) and hypothalamus in humans (6). Though ^{11}C -(+)-PHNO is not a perfectly selective D_3R radioligand, it is, to date, the most specific radioligand available to assess D_3R in vivo in humans (7).

Kinetic modeling of ^{11}C -(+)-PHNO has been performed previously in humans (8): for studies with arterial blood sampling, a constrained form of the two-tissue compartment (2TC) model was selected as the method of choice to estimate BP_{ND} binding potentials, and for studies without arterial blood sampling, the simplified reference tissue model (SRTM) provided highly correlated outcomes (albeit with a 10% underestimation of BP_{ND}). One goal of the present study was to evaluate the test-retest variability (TRV) of ^{11}C -(+)-PHNO parameter estimates using a within-day design and the high resolution PET scanner, HRRT. The latter is especially relevant in light of the regional D_3R specificity of small structures, such as the SN. The second goal of this study was to evaluate strategies for computing parametric images of ^{11}C -(+)-PHNO binding potentials in order to minimize image noise while using the lowest amount of spatial smoothing possible, for purposes of elucidating receptor topology at high resolution. In addition, potential mass carryover effect on binding parameters, as seen in previous pre-clinical studies (9), was also investigated in this within-day, repeated-scan paradigm, particularly in high-affinity D_3R -rich regions.

MATERIALS AND METHODS

Subjects

Eight subjects (7 male, 1 female) were included in the study: five were healthy controls (HC) and three were cocaine dependent (CD) according to the Diagnostic and Statistical Manual of Mental Disorders, fourth edition (DSM-IV; American Psychiatric Press, 1994) criteria. We purposefully included a patient group in the test-retest (T-R) assessment (see Discussion). The average age and weight were 35 ± 9 years and 80 ± 16 kg, respectively. The absence of recent substance use was confirmed by urine toxicology on both the day of screening and the PET scan day, prior to tracer injection.

The study was performed under protocols approved by the Yale School of Medicine Human Investigation Committee, the Human Subjects Subcommittee of the Veterans Affairs Connecticut Healthcare System, the Yale-New Haven Hospital Radiation Safety Committee, and the Yale University Radiation Safety Committee. Subjects were recruited by public advertisement. Written informed consent was obtained from all participants after full explanation of study procedures.

Radiochemistry

^{11}C -(+)-PHNO was prepared by *N*-acylation of the norpropyl precursor with ^{11}C -propionyl chloride followed by reduction of the resulting amide with lithium aluminum hydride and purification by reverse-phase HPLC, in a modified literature procedure (1). See supplemental information for details. The radiochemical and chemical purity were >98% and >99%, respectively, and the specific activity at the end of synthesis was 83 ± 35 MBq/nmol.

PET Imaging

Each subject underwent two PET scans on the same day, separated by 5.4 ± 0.7 hours (min=4.5 hours), on the High Resolution Research Tomograph (HRRT) (Siemens/CTI, Knoxville, TN, USA). 328 ± 103 MBq of ^{11}C -(+)-PHNO was injected by a computer-controlled infusion pump (Harvard PHD 22/2000, Harvard Apparatus, Holliston, Massachusetts, United States). The tracer specific activity at time of injection was 45 ± 18 MBq/nmol. The injected mass was 25 ± 5 ng/kg (max 31 ng/kg). The injected dose, injected mass, and specific activity did not differ significantly between the test and retest scans (paired t-test, $p=0.13$, 0.97 and 0.60 , respectively) (Table 1). The metabolite-corrected arterial input function and the plasma free fraction (f_p) of ^{11}C -(+)-PHNO were measured. See supplemental information for details.

Quantification of PET Data

Gray matter regions-of-interest (ROIs) were taken from the Anatomical Automatic Labeling (AAL) template. Six ROIs were selected: cerebellum, caudate, putamen, pallidum, amygdala, and thalamus. Extra ROIs corresponding to the hypothalamus and ventral striatum were also drawn on the template MRI, and a substantia nigra (SN) template ROI was also created based on PET images (see supplemental information). The template ROIs were applied to the PET data using non-linear transforms (see supplemental information).

Based on a previous report (8), the two-tissue compartment (2TC) model and multilinear analysis (MA1) method (10) were evaluated to quantify the volume of distribution (V_T) (11) using arterial blood sampling. To compare between 1TC and 2TC quality of fit, the residual sum of square was compared using the F-test, using cut-off p-value of 0.05 corrected for the number of comparisons (i.e., the number of scans, 16). For MA1, the starting time of the fit, t^* , was set to 30 min. Based on the V_T values, three versions of the binding potential (BP_F , BP_P , and BP_{ND}) (11) were calculated, with the cerebellum used as the reference region. In addition, the Simplified Reference Tissue Model (SRTM) (12) was used to estimate ^{11}C -(+)-PHNO BP_{ND} without arterial blood sampling.

For parametric imaging, both the SRTM (12) and SRTM2 (13) methods were tested. Both SRTM and SRTM2 were implemented using a basis-function approach restricting the parameter k_2 (the clearance rate constant of each voxel) to the range of 0.01–1.0 min⁻¹. No spatial smoothing was applied. In SRTM2, the clearance rate constant of the reference region, k_2' , was estimated from SRTM parametric images, as the median k_2' estimate from brain voxels where $BP_{ND} > 0.5$. ROIs, as described above, were applied to the parametric images, and the mean values for BP_{ND} were compared to those obtained by fits of regional TACs.

Test-Retest Variability Estimation

Test-retest variability (TRV) was estimated for each parameter of interest p by computing first Δp as defined below:

$$\Delta p = 2 \frac{p^{\text{retest}} - p^{\text{test}}}{p^{\text{retest}} + p^{\text{test}}} \quad (\text{Eq. 1})$$

and then by computing the means of Δp across subjects (noted as $m(\Delta p)$) and the standard deviation of Δp across subjects (noted as $\sigma(\Delta p)$), with $m(\Delta p)$ indicating whether there is a trend between the two scans for the parameter of interest p , and $\sigma(\Delta p)$ as an index of the variability for the estimates of the parameter of interest p . An alternate index of the variability for the estimates of the parameter of interest p was also computed as the mean across subjects of the absolute value of Δp , and noted as $m(|\Delta p|)$. For comparison with a previous study (14), $\sigma(\delta p)$ was computed, where $\delta p = (p^{\text{retest}} - p^{\text{test}})/p^{\text{test}}$. Finally, the intraclass correlation coefficient (ICC) was also computed as in (15). Note that, since this study includes HC and CD subjects, the between-subject variance is larger than what would be present in a single-group study; this will cause the ICC values to be increased (see Discussion).

For parametric images, TRV was computed in two ways: first, to estimate variability in ROI-based analyses, TRV was computed using the regional averages of the parametric images. Then, to assess variability for statistical analyses of parametric images, test and retest parametric images were resliced to the ROI template space, images of $\sigma(\Delta p)$ and $m(|\Delta p|)$ were generated in template space, and finally the median of $\sigma(\Delta p)$ and $m(|\Delta p|)$ within each ROI was computed.

RESULTS

Kinetic Analysis with Arterial Input Function

In the pallidum, hypothalamus, ventral striatum and SN, the 2TC model provided better fits than the one-tissue compartment (1TC) model for all subjects and scans (F test, $p < 0.003$). In other regions, 2TC provided better fits for the majority of scans. However, 2TC did not provide reliable V_T estimates in most regions, with at least 25% of the V_T relative standard errors (%SE) being higher than 50% in the cerebellum, putamen, ventral striatum, hypothalamus and SN, and ICC values being for V_T estimates being lower than 0.03.

Due to the variability in 2TC V_T estimates, MA1 was also evaluated. Typical fits obtained with MA1, 1TC, and 2TC models, are shown in Figure 1. For the subset of regions and scans for which the 2TC V_T %SE was lower than 5%, the V_T values estimated with MA1 ($t^*=30$ min) and 2TC were nearly identical ($r^2=0.996$, $y=0.97x+0.17$, where x represents the 2TC estimates and y represents the MA1 estimates). With MA1, the %SE of V_T was less than 5% for all scans in the amygdala, caudate, putamen, pallidum and thalamus. In the SN, ventral striatum and hypothalamus the highest %SE were 12%, 7% and 12%, respectively.

The MA1 parameter estimates from the test scan for HC subjects ($n=5$), and the T-RT statistics for all subjects ($n=8$) are listed in Table 2. There were no significant differences between test and retest V_T in any ROI (paired t-test; p-value from 0.37 to 0.92), and the mean relative change of V_T , $m(|V_T|)$, ranged between -9% and +2%. The variability of V_T ($\sigma(V_T)$) ranged from 13% in putamen to 25% in SN. The means of the absolute values of V_T , $m(|V_T|)$, were lower than $\sigma(V_T)$ and ranged from 9% to 21% (see Discussion). The ICC values for V_T estimates ranged from 0.28 in the cerebellum to 0.88 in the pallidum. The plasma free fraction (f_p) was 0.44 ± 0.03 ($n=5$) for the test scans, with no T-RT change ($f_p = 0\pm 7\%$, $n = 8$; p-value = 0.88, paired t-test; $m(|f_p|) = 5\%$). Normalizing V_T by f_p did not change TRV (See supplemental file). $\sigma(BP_{ND})$ ranged from 10% to 29%, and $m(|BP_{ND}|)$ ranged from 6% to 25%. The variability of BP_P and BP_F was ~22% and ~13% higher, respectively, than that of BP_{ND} (based on $\sigma(p)$) (See supplemental file). The ICC values for MA1 BP_{ND} estimates ranged from 0.29 in the amygdala to 0.92 in SN and caudate.

Kinetic Analysis with Reference Region

SRTM BP_{ND} in the caudate, putamen, pallidum and SN were well correlated with BP_{ND} estimated with MA1. The parameters of the regression line between MA1 and SRTM BP_{ND} values were: slope= 0.966 ± 0.012 , intercept= 0.080 ± 0.032 , $r^2=0.984$). Thalamus was not included in this comparison since SRTM BP_{ND} estimates in thalamus had very poor identifiability (max %SE >100%; $BP_{ND} = 1\pm 105\%$). TRV indices for SRTM BP_{ND} are listed in Table 3. The variability of SRTM BP_{ND} estimates was very similar to that of MA1 BP_{ND} estimates in the basal ganglia and SN (neither BP_{ND} nor $|BP_{ND}|$ were significantly different between these two methods in these ROIs: paired Student t-test p-values >0.11). The ICC values for SRTM BP_{ND} estimates ranged from 0.06 in the hypothalamus to 0.92 in the caudate.

Parametric Imaging

Typical SRTM and SRTM2 parametric images are shown in Figure 2. Visually, SRTM and SRTM2 BP_{ND} images are very similar, with slightly lower noise in SRTM2 images (noise reduction is more visible in low binding regions or near high BP_{ND} areas), but also slightly lower BP_{ND} values in D_3 -rich regions. There was a visually bigger reduction of noise with SRTM2 for delivery (R_1) images. The variability of the parametric images was quantified by computing parametric images of $\sigma(R_1)$ and $\sigma(BP_{ND})$ in template space. The median value in each ROI is reported in Table S3 of the supplemental information file. The median of $\sigma(R_1)$ ranged from 20% to 37% with SRTM, and from 14% to 23% for SRTM2, and the improvement with SRTM2 ranged from 2 percentage points (in SN) to 14 percentage points (in amygdala). The median of $\sigma(BP_{ND})$ ranged from 34% (in caudate) to 155% (in

amygdala) with SRTM, and from 22% (in caudate) to 86% (in amygdala) with SRTM2, and the improvement with SRTM2 ranged from -1 percentage point in hypothalamus to 69 percentage points in amygdala.

ROI values from the parametric images were well correlated with BP_{ND} estimated from fits of regional TACs. The regression parameters between MA1 and parametric BP_{ND} were slope= 0.888 ± 0.018 , intercept= 0.219 ± 0.047 and $r^2=0.952$ for SRTM, and slope= 0.861 ± 0.019 , intercept= 0.133 ± 0.048 and $r^2=0.941$ for SRTM2. At the regional average level, SRTM2 and SRTM BP_{ND} were very highly correlated (slope= 0.971 ± 0.009 , intercept= -0.081 ± 0.021 and $r^2=0.990$), though SRTM2 values were slightly lower than SRTM values, with relative differences ranging from $0\pm 2\%$ in putamen to $-19\pm 7\%$ hypothalamus, with $-12\pm 8\%$ in SN (significant in all regions except putamen).

TRV indices and ICC values of regional averages from SRTM and SRTM2 parametric images are listed in Table 4. The variability of SRTM and SRTM2 values was similar to that of MA1 BP_{ND} estimates in all ROIs.

Carry-Over Mass Effect

There were no significant differences between test and retest BP_{ND} in any ROI outside of the SN (paired t-test; p-value 0.14–0.95). In SN, there was a trend level or significant reduction in BP_{ND} in the retest scans depending on the method. The p values were 0.06 with MA1 and <0.05 with SRTM and parametric SRTM and SRTM2 (paired t-test; n = 8). The average reduction of the SN BP_{ND} across all methods was $-14\pm 15\%$.

DISCUSSION

The current study extends evaluations of optimal image and data analyses for ^{11}C -(+)-PHNO bolus injection PET studies in human using multiple modeling methods, parametric imaging, and T-RT studies. A detailed comparison of kinetic modeling methods for quantifying ^{11}C -(+)-PHNO binding in humans has been published previously (8). In that study, the 2TC model was the method of choice to estimate ^{11}C -(+)-PHNO volume of distribution. However, in the current study, high %SE was observed in some scans and regions of interest. The differences between these two studies may also be due to different noise properties of the two data sets (both were acquired on the same type of scanner, but with different reconstruction algorithms), differences in the delineation of the regions of interest, or differences in the fitting routines and settings.

A method providing a compromise between 2TC's quality of fit and the stability of V_T estimates was needed. The Logan graphical analysis was tested in the previous study and was found to provide V_T estimates highly correlated to, and not statistically different from, those obtained using unconstrained 2TC fits (8). However, the Logan graphical analysis is sensitive to noise, especially for small regions or single-voxel TACs. The multilinear analysis MA1, which was designed to reduce this bias (10), was tested and proved to be the preferred method, as it provided more stable parameter estimates than 2TC.

In theory, SRTM is not a valid method for $^{11}\text{C-}(+)\text{-PHNO}$ since the regional TACs are not well fitted with the 1TC model when the arterial input function is used. However, SRTM provided BP_{ND} estimates in good agreement with the MA1 estimates. This is partially in agreement with the earlier results (8): SRTM BP_{ND} estimates were in good agreement with BP_{ND} estimates with unconstrained 2TC fits (method B in (8)), but they were lower than BP_{ND} estimates from constrained 2TC fits (method D in (8)), the latter being the method of choice in that study. However, in the current study the good correlation between MA1 and SRTM BP_{ND} estimates was verified in a larger selection of regions of interest, adding the SN, amygdala and hypothalamus. SRTM2 also provided BP_{ND} estimates in good agreement with MA1 estimates.

In this study, two TRV indices were computed: $m(|p|)$ and $\sigma(p)$. The main advantage of computing the mean and standard deviation of p ($m(p)$ and $\sigma(p)$) is that it can be used to assess whether there is a systematic trend or significant change in binding parameters between the test and retest scans. Computing only $m(|p|)$ does not permit the assessment of that trend. However, $m(|p|)$ and $\sigma(p)$ tend to provide numerically different indices for the variability of the parameter p , with $\sigma(p)$ being typically higher than $m(|p|)$. Indeed, for a Gaussian variable p , with no trend between the test and retest scans (i.e., $m(p) = 0$), $m(|p|)$ is close to the relative standard deviation of p , while $\sigma(p)$ is higher than the relative standard deviation of p by a factor 2, since it represents the combined errors in the test and retest scans. On the other hand, $\sigma(p)$ will be close to the standard deviation of p obtained in studies comparing baseline to post-intervention scans, when the effect of the intervention is small. Thus, $\sigma(p)$ is useful to evaluate the possibility to detect small differences or effects. However, $m(|p|)$ is frequently used in the literature and, thus, is useful to compute in addition to $\sigma(p)$ when comparing tracers or methods.

Due to the high affinity of $^{11}\text{C-}(+)\text{-PHNO}$ for D3R and prior suggestions that PET studies performed using 0.03 $\mu\text{g}/\text{kg}$ of $^{11}\text{C-}(+)\text{-PHNO}$ may not actually occur under true tracer conditions (5, 16), it was postulated that binding potential estimates would be lower in D₃-rich regions during the same-day retest scanning. This was seen in a previous pre-clinical study (9), where the injected mass of $^{11}\text{C-}(+)\text{-PHNO}$ was $\sim 0.04 \mu\text{g}/\text{kg}$ and the delay between injections was ~ 3 hours and $m(\delta BP_{\text{ND}})$ ranged from -22% to -42% in D₃-rich regions. The current study was not designed to maximize chances of observing a carry-over mass effect, but rather, to evaluate if such an effect could be detected despite the deliberate use of a longer (5-hour) interval between $^{11}\text{C-}(+)\text{-PHNO}$ injections. As postulated, a significant reduction in BP_{ND} was detected in the SN in the retest scans, though this reduction was not significant with all methods, and would not survive correction for multiple comparisons. The average $m(BP_{\text{ND}})$ was -14% across all methods. Three mechanisms for this carry-over effect are possible. First, sufficient unlabeled (+)-PHNO from the first injection might remain and compete for tracer binding during the second injection. Second, receptor changes in response to non-tracer doses of the agonist during scan one are also possible (albeit unlikely here). Finally, we cannot rule-out potential differences resulted from circadian variations, since by design all initial injections were around 10 am and all second injections around 3 to 4 pm. The first hypothesis is compatible with estimates of the remaining concentration of (+)-PHNO during the second scan and previous estimates of $^{11}\text{C-}(+)\text{-}$

PHNO ED_{50} . Indeed, during the first scan, the observed BP_{ND} would be given by the following equation:

$$BP_{ND}^T = BP_{ND}^0 \times \left(1 - \frac{C}{C + IC_{50}}\right) \quad (\text{Eq. 2})$$

where BP_{ND}^0 is the true binding potential at tracer dose, C is the concentration of tracer in tissue and IC_{50} is the concentration of tracer to induce 50% reduction in binding. During the retest scan, assuming that the injected dose is similar, the observed BP_{ND} would be:

$$BP_{ND}^R = BP_{ND}^0 \times \left(1 - \frac{C \times (1+f)}{C \times (1+f) + IC_{50}}\right) \quad (\text{Eq. 3})$$

where f is the fraction of tracer remaining from the first injection. Between the end of first scan and the beginning of the second, concentration of free (+)-PHNO in SN may have decreased by 64%, based on extrapolation of the cerebellum curve, to 48%, based on extrapolation of the SN curve. To observe a mean BP_{ND} value of 14% in such conditions, the concentration C in the above equations would need to be ~50% of the tracer IC_{50} . The average dose of ^{11}C -(+)-PHNO used in this study was 25 ng/kg, which is indeed close to 50% of the ^{11}C -(+)-PHNO ED_{50} estimated in a previous study (40 ng/kg) (16). While there was no significant difference in the hypothalamus, another region where ~100% of ^{11}C -(+)-PHNO BP_{ND} is due to D3R binding, there was, nonetheless, a similar trend ($m(BP_{ND})$ of -10% in average across all methods), which was not significant due to the higher variability of ^{11}C -(+)-PHNO BP_{ND} in this region.

Comparing the various methods of computing BP_{ND} , the variability of MA1 and SRTM estimates was comparable for ROI TAC analyses, except in the thalamus, where SRTM results were quite unreliable. Using regional averages from parametric images, the variability of SRTM and SRTM2 BP_{ND} values was slightly lower than that of MA1 estimates. This effect was attributed to the choice of basis functions, which acted like a filter or a prior (see discussion below about parametric images). The ICC criterion leads to a similar conclusion: ICC values were slightly lower for SRTM BP_{ND} estimates than for MA1 BP_{ND} estimates, while ICC values for BP_{ND} values from parametric images (SRTM or SRTM2) were closer to the ICC values for MA1 BP_{ND} estimates.

The TRV of ^{11}C -(+)-PHNO BP_{ND} estimated with SRTM in this study was slightly better (lower) than in a previous study (14) for caudate and putamen ($\sigma(\delta BP_{ND})$ was 9–10%, versus 12% in the previous study) and much lower for pallidum ($\sigma(\delta BP_{ND})$ was 11% versus 28% in the previous study). Conversely, the TRV of BP_{ND} estimated with SRTM in this study was slightly higher ($\sigma(BP_{ND})$ was 2 ± 4 percentage points higher on average for caudate, putamen, pallidum, ventral striatum and SN) than the variability of BP_{ND} estimated by equilibrium analysis (EA) using a bolus/infusion protocol (19).

In comparison to other tracers, the TRV of ^{11}C -(+)-PHNO V_T estimates was higher than that of ^{11}C -raclopride: $m(|V_T|)$ was 12% and 10% in the cerebellum and caudate/putamen for ^{11}C -(+)-PHNO, vs. 9% for ^{11}C -raclopride (20). Similarly, the TRV of ^{11}C -(+)-PHNO

BP_{ND} was higher than that of ^{11}C -raclopride: $m(|BP_{ND}|)$ of 9% for ^{11}C -(+)-PHNO in caudate/putamen vs. only 4–6% for ^{11}C -raclopride (21).

Compared to other D2R/D3R agonist radioligands, the TRV of ^{11}C -(+)-PHNO was also greater than that for ^{11}C -NPA, where $m(|V_T|)$ was 6–9% and $m(|BP_{ND}|)$ was 4–10%, depending on region. (18). Compared to ^{11}C -MNPA (22), ^{11}C -(+)-PHNO $m(|BP_{ND}|)$ was higher in putamen (9% vs. 5%) and lower in caudate (8% vs. 12%).

Parametric images were computed using SRTM and SRTM2 with a basis function approach. Due to the relatively rapid kinetics of ^{11}C -(+)-PHNO, it was possible to obtain low noise parametric images with both methods without spatial smoothing by restricting the range of the basis functions (restricting k_2 to be $>0.01 \text{ min}^{-1}$). Indeed, the basis functions used in the SRTM model are of the form $C_R(t) \otimes e^{-k_2 t}$, where $C_R(t)$ is the reference region TAC. We chose to limit the k_2 values based on results of ROI TAC analyses with SRTM2. Due to this restriction, SRTM parametric BP_{ND} images had relatively low noise, and the simplified model, SRTM2, mostly improved flow images (R_1) and BP_{ND} images outside of the main regions of interest.

In this T-RT study, we intentionally included subjects who were not HC subjects. Including such subjects helped to insure that the selected methods are applicable without major increases in TRV in subjects that may have “atypical” binding, since either higher or lower BP_{ND} in some regions can have an impact on the variability of the measures. On average, across all ROIs, the ratio of $m(|BP_{ND}|)$ in CD and in HC subjects was 1.02, indicating that there was no global difference in variability between the two groups. The inclusion of non-control subjects can however have a bigger impact on ICC than TRV, since the ICC value is sensitive, by design, to the variability across subjects, which may be increased by including non-control subjects. This sensitivity of ICC to the study population does not prevent its use as a criterion to compare quantification methods, but can be an issue when comparing results between studies on different populations (by diagnosis, age or other demographic criteria influencing binding).

CONCLUSION

The TRV of ^{11}C -(+)-PHNO binding potential was 9% in caudate and putamen, which is good, though higher than that of the leading antagonist, ^{11}C -raclopride, and other available agonists, including ^{11}C -NPA and ^{11}C -MNPA. Parametric images of ^{11}C -(+)-PHNO can be computed with low noise using both SRTM and SRTM2.

Supplementary Material

Refer to Web version on PubMed Central for supplementary material.

Acknowledgments

We would like to thank the staff of the Clinical Neuroscience Research Unit (CNRU) at Connecticut Mental Health Center (CMHC). This work was supported by a NARSAD Young Investigator Award Grant (M132018; DM), the National Institute on Drug Abuse (NIDA) (K24 DA017899; 1R03DA027456-01; RTM), the National Institute of Mental Health (NIMH; T32 MH019961; DM/RTM), Yale PET Center, and YCCI Pilot Projects Utilizing Core

Technologies and the Department of Mental Health and Addiction Services (DMHAS) of the State of Connecticut. This publication was also made possible by CTSA Grant Number UL1 RR024139 from the National Center for Research Resources (NCRR) and the National Center for Advancing Translational Science (NCATS), components of the National Institutes of Health (NIH).

References

1. Wilson AA, McCormick P, Kapur S, et al. Radiosynthesis and evaluation of [^{11}C]-(+)-4-propyl-3,4,4a,5,6,10b-hexahydro-2H-naphtho[1,2-b][1,4]oxazin-9-ol as a potential radiotracer for in vivo imaging of the dopamine D2 high-affinity state with positron emission tomography. *J Med Chem.* 2005; 48:4153–4160. [PubMed: 15943487]
2. Willeit M, Ginovart N, Kapur S, et al. High-affinity states of human brain dopamine D2/3 receptors imaged by the agonist [^{11}C]-(+)-PHNO. *Biol Psychiatry.* 2006; 59:389–394. [PubMed: 16373068]
3. Narendran R, Slifstein M, Guillin O, et al. Dopamine (D2/3) receptor agonist positron emission tomography radiotracer [^{11}C]-(+)-PHNO is a D3 receptor preferring agonist in vivo. *Synapse.* 2006; 60:485–495. [PubMed: 16952157]
4. Freedman SB, Patel S, Marwood R, et al. Expression and pharmacological characterization of the human D3 dopamine receptor. *J Pharmacol Exp Ther.* 1994; 268:417–426. [PubMed: 8301582]
5. Gallezot J-D, Beaver JD, Gunn RN, et al. Affinity and selectivity of [^{11}C]-(+)-PHNO for the D3 and D2 receptors in the rhesus monkey brain in vivo. *Synapse.* 2012; 66:489–500. [PubMed: 22213512]
6. Tziortzi AC, Searle GE, Tzimopoulou S, et al. Imaging dopamine receptors in humans with [^{11}C]-(+)-PHNO: dissection of D3 signal and anatomy. *Neuroimage.* 2011; 54:264–277. [PubMed: 20600980]
7. Rabiner EA, Laruelle M. Imaging the D3 receptor in humans in vivo using [^{11}C]-(+)-PHNO positron emission tomography (PET). *Int J Neuropsychopharmacol.* 2010; 13:289–290. [PubMed: 20149269]
8. Ginovart N, Willeit M, Rusjan P, et al. Positron emission tomography quantification of [^{11}C]-(+)-PHNO binding in the human brain. *J Cereb Blood Flow Metab.* 2007; 27:857–871. [PubMed: 17033687]
9. Girgis RR, Xu X, Miyake N, et al. In vivo binding of antipsychotics to D(3) and D(2) receptors: a PET study in baboons with [(11)C]-(+)-PHNO. *Neuropsychopharmacology.* 2011; 36:887–895. [PubMed: 21178982]
10. Ichise M, Toyama H, Innis RB, Carson RE. Strategies to improve neuroreceptor parameter estimation by linear regression analysis. *J Cereb Blood Flow Metab.* 2002; 22:1271–1281. [PubMed: 12368666]
11. Innis RB, Cunningham VJ, Delforge J, et al. Consensus nomenclature for in vivo imaging of reversibly binding radioligands. *J Cereb Blood Flow Metab.* 2007; 27:1533–1539. [PubMed: 17519979]
12. Lammertsma AA, Hume SP. Simplified reference tissue model for PET receptor studies. *Neuroimage.* 1996; 4:153–158. [PubMed: 9345505]
13. Wu Y, Carson RE. Noise reduction in the simplified reference tissue model for neuroreceptor functional imaging. *J Cereb Blood Flow Metab.* 2002; 22:1440–1452. [PubMed: 12468889]
14. Willeit M, Ginovart N, Graff A, et al. First human evidence of d-amphetamine induced displacement of a D2/3 agonist radioligand: A [^{11}C]-(+)-PHNO positron emission tomography study. *Neuropsychopharmacology.* 2008; 33:279–289. [PubMed: 17406650]
15. Shrout PE, Fleiss JL. Intraclass Correlations: Uses in Assessing Rater Reliability. *Psychol Bull.* 1979; 86:420–428. [PubMed: 18839484]
16. Searle GE, Beaver JD, Tziortzi A, et al. Mathematical modelling of [^{11}C]-(+)-PHNO human competition studies. *Neuroimage.* 2013; 68:119–132. [PubMed: 23207573]
17. Mawlawi O, Martinez D, Slifstein M, et al. Imaging human mesolimbic dopamine transmission with positron emission tomography: I. Accuracy and precision of D(2) receptor parameter measurements in ventral striatum. *J Cereb Blood Flow Metab.* 2001; 21:1034–1057. [PubMed: 11524609]

18. Narendran R, Frankle WG, Mason NS, et al. Positron emission tomography imaging of D(2/3) agonist binding in healthy human subjects with the radiotracer [(11)C]-N-propyl-norapomorphine: preliminary evaluation and reproducibility studies. *Synapse*. 2009; 63:574–584. [PubMed: 19301416]
19. Lee DE, Gallezot J-D, Zheng M-Q, et al. Test-retest reproducibility of [¹¹C]-(+)-propyl-hexahydro-naphtho-oxazin positron emission tomography using the bolus plus constant infusion paradigm. *Mol imaging*. 2013; 12:77–82. [PubMed: 23415395]
20. Logan J, Volkow ND, Fowler JS, et al. Effects of blood flow on [¹¹C]raclopride binding in the brain: model simulations and kinetic analysis of PET data. *J Cereb Blood Flow Metab*. 1994; 14:995–1010. [PubMed: 7929663]
21. Alakurtti K, Aalto S, Johansson JJ, et al. Reproducibility of striatal and thalamic dopamine D2 receptor binding using [¹¹C]raclopride with high-resolution positron emission tomography. *J Cereb Blood Flow Metab*. 2011; 31:155–165. [PubMed: 20442726]
22. Kodaka F, Ito H, Kimura Y, et al. Test-retest reproducibility of dopamine D2/3 receptor binding in human brain measured by PET with [¹¹C]MNPA and [¹¹C]raclopride. *Eur J Nucl Med Mol Imaging*. 2013; 40:574–579. [PubMed: 23238524]

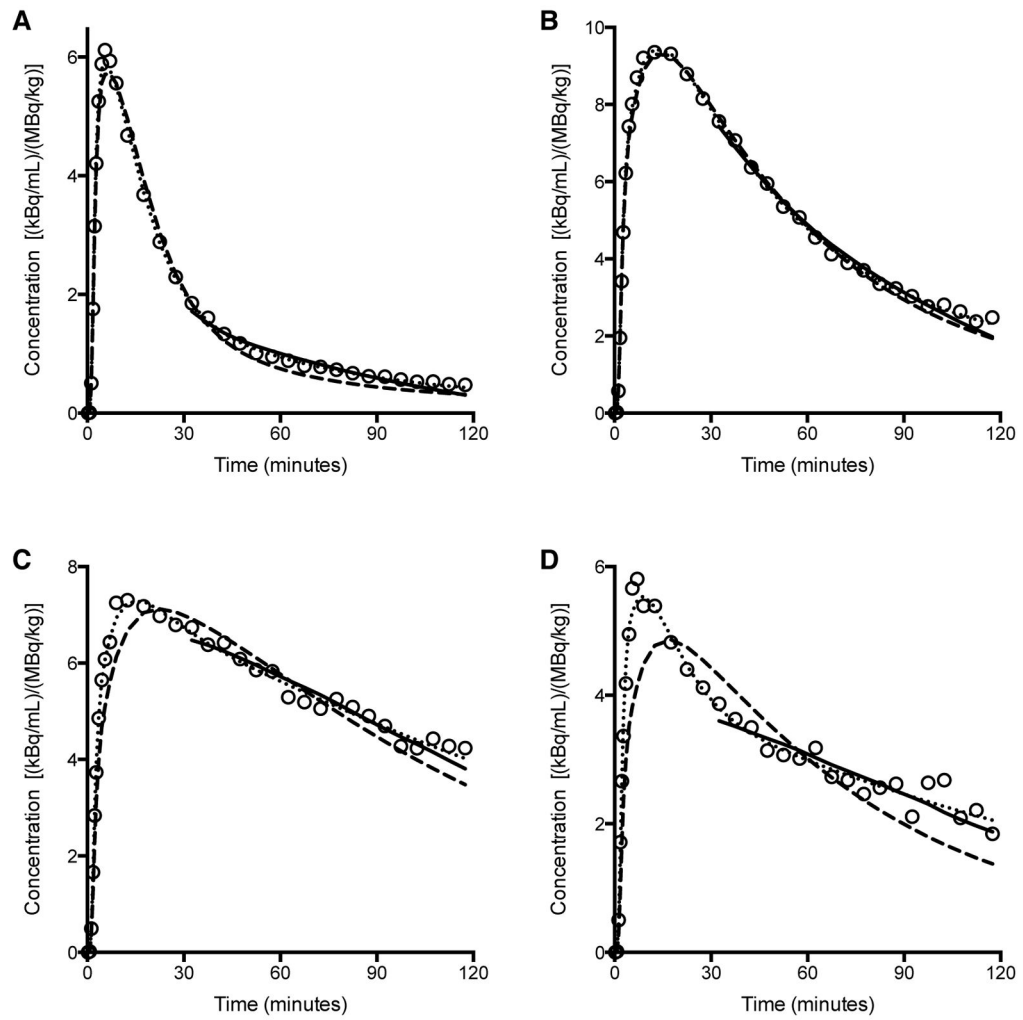


Figure 1. Sample fits obtained with MA1 (solid line), and with the 1TC (dashed line) and 2TC (dotted line) models in one typical subject's test scan. Data are derived from SUV values in **A**. Cerebellum, **B**. Putamen, **C**. Pallidum, and **D**. Substantia Nigra.

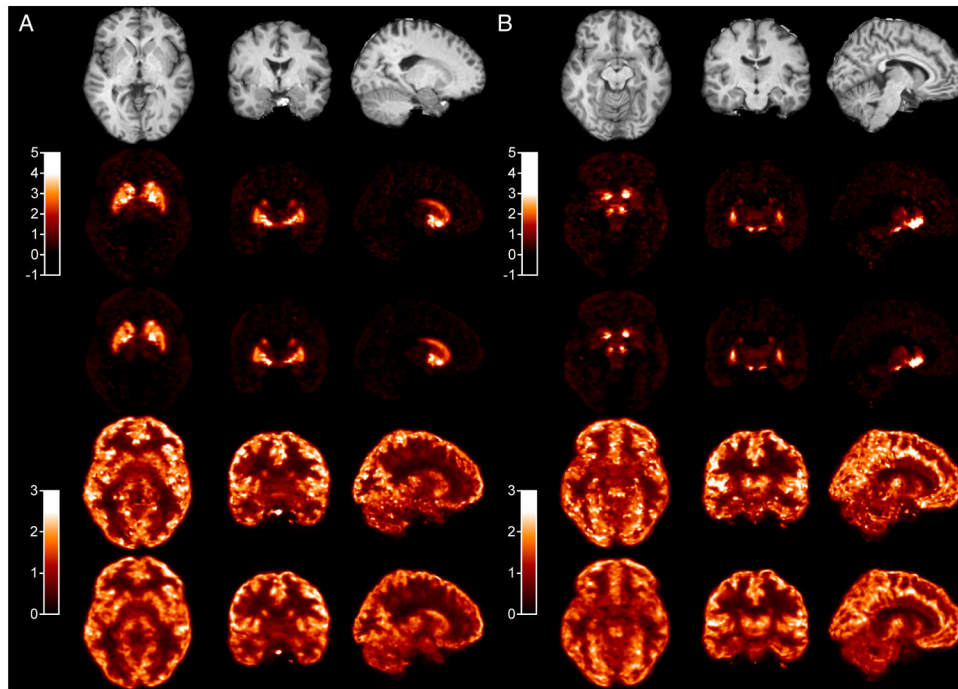


Figure 2. Typical parametric images at the level of the pallidum (**A**) and substantia nigra (**B**). Row 1: Co-registered MR. Row 2: SRTM BP_{ND} . Row 3: SRTM2 BP_{ND} . Row 4: SRTM R_1 (relative delivery). Row 5: SRTM2 R_1

Table 1

Synthesis and injection parameters.

	Test Scan	Retest Scan	Variation *
Specific Activity at End of Synthesis (MBq/nmol)	76±30	90±38	27%±57%
Specific Activity at Time of Injection (MBq/nmol)	42±17	47±17	25%±58%
Injected Dose (MBq)	315±111	342±93	13%±19%
Injected Mass (ng/kg)	25±5	25±6	6%±39%

* Computed as retest value/test value – 1.

Table 2

V_T and BP_{ND} estimates for MA1 fits of regional TACs.

	V_T			BP_{ND}		
	Average*	V_T^{\dagger}	ICC ‡	Average*	BP_{ND}^{\S}	ICC ‡
Cerebellum	4.7±0.7(14%)	2%±18%(12%)	0.28[-0.44;0.79]			
Caudate	13.2±1.8(14%)	0%±15%(11%)	0.81[0.35;0.96]	1.8±0.2(9%)	-2%±10%(9%)	0.92[0.69;0.98]
Putamen	15.8±1.9(12%)	-1%±13%(9%)	0.72[0.16;0.94]	2.4±0.2(8%)	-4%±11%(9%)	0.57[-0.11;0.89]
Pallidum	20.1±3.2(16%)	-2%±14%(9%)	0.88[0.54;0.97]	3.3±0.6(17%)	-6%±11%(6%)	0.87[0.51;0.97]
V. Striatum	22.2±4.9(22%)	0±21%(15%)	0.64[0.01;0.92]	3.7±0.6(15%)	-2±12%(10%)	0.82[0.38;0.96]
Amygdala	5.9±0.8(14%)	-1±15%(10%)	0.51[-0.19;0.88]	0.26±0.07(26%)	-13±29%(25%)	0.29[-0.42;0.80]
Sub. Nigra	13.4±2.6(19%)	-9%±25%(21%)	0.85[0.45;0.97]	1.8±0.4(19%)	-16%±17%(19%)	0.92[0.68;0.98]
Thalamus	6.4±1.2(18%)	2%±17%(13%)	0.55[-0.13;0.89]	0.36±0.10(28%)	2%±19%(14%)	0.73[0.17;0.94]
Hypothalamus	12.4±2.7(22%)	-3%±14%(11%)	0.80[0.32;0.95]	1.7±0.8(48%)	-7%±27%(21%)	0.55[-0.14;0.89]

* n=5 healthy controls; data are presented as mean±sd (relative sd) across subjects.

† n=8 subjects; data are presented as $m(V_T) \pm \alpha(V_T)$ ($m(V_T)$ (lower bound); $\alpha(V_T)$ (upper bound)).

‡ n=8 subjects; ICC is presented as estimate [lower bound; upper bound] of 95% confidence interval.

§ n=8 subjects; data are presented as $m(BP_{ND}) \pm \alpha(BP_{ND})$ ($m(BP_{ND})$ (lower bound); $\alpha(BP_{ND})$ (upper bound)).

Table 3

BP_{ND} estimates for SRTM fits of regional TACs.

	Average *	BP_{ND} †	ICC ‡
Caudate	1.8±0.1(8%)	-3%±9%(8%)	0.92[0.70;0.98]
Putamen	2.4±0.2(8%)	-4%±10%(9%)	0.59[-0.07;0.90]
Pallidum	3.3±0.6(18%)	-4%±12%(8%)	0.81[0.36;0.96]
V. Striatum	3.6±0.4(12%)	-1%±13%(12%)	0.74[0.20;0.94]
Amygdala	0.29±0.16(54%)	-22%±41%(36%)	0.15[-0.54;0.74]
Sub. Nigra	2.0±0.3(13%)	-19%±18%(20%)	0.86[0.50;0.97]
Thalamus	0.38±0.11(29%)§	1%±105%(71%)	0.33[-0.39;0.81]
Hypothalamus	2.6±2.5(95%)	-14%±54%(38%)	0.06[-0.60;0.69]

* n=5 healthy controls; data are presented as mean±sd (relative sd) across subjects.

† n=8 subjects; data are presented as $m(BP_{ND}) \pm \alpha(BP_{ND})$ ($m()$ (BP_{ND})).

‡ n=8 subjects; ICC is presented as estimate [lower bound; upper bound] of 95% confidence interval.

§ excluding one outlier

Table 4

Regional BP_{ND} values from parametric maps.

	SRTM			SRTM2		
	Average*	BP_{ND}^{\ddagger}	ICC [‡]	Average*	BP_{ND}^{\ddagger}	ICC [‡]
Caudate	2.0±0.1(7%)	-3%±9%(8%)	0.92[0.68;0.98]	1.9±0.2(10%)	-3%±10%(9%)	0.91[0.65;0.98]
Putamen	2.6±0.2(8%)	-4%±11%(9%)	0.63[-0.01;0.91]	2.5±0.2(9%)	-4%±11%(9%)	0.59[-0.07;0.90]
Pallidum	3.3±0.5(15%)	-4%±11%(7%)	0.76[0.23;0.95]	3.2±0.6(18%)	-5%±12%(8%)	0.76[0.24;0.95]
V. Striatum	3.8±0.4(10%)	-1%±11%(9%)	0.80[0.33;0.96]	3.5±0.5(13%)	-2%±12%(8%)	0.80[0.34;0.96]
Amygdala	0.32±0.07(23%)	-11%±24%(21%)	0.32[-0.40;0.81]	0.27±0.08(28%)	-12%±28%(24%)	0.30[-0.42;0.80]
Sub. Nigra	1.8±0.3(16%)	-9%±12%(11%)	0.94[0.77;0.99]	1.6±0.4(24%)	-11%±14%(12%)	0.95[0.79;0.99]
Thalamus	0.40±0.12(29%)	-1%±21%(15%)	0.71[0.14;0.93]	0.36±0.09(25%)	-1%±20%(15%)	0.50[-0.20;0.87]
Hypothalamus	1.6±0.6(36%)	-8%±22%(17%)	0.54[-0.15;0.88]	1.3±0.6(46%)	-9%±21%(16%)	0.61[-0.05;0.91]

* n=5 healthy controls; data are presented as mean±sd (relative sd) across subjects.

† n=8 subjects; data are presented as $m(BP_{ND}) \pm \alpha(BP_{ND})$ ($m(BP_{ND})$ ($m(BP_{ND})$)).

‡ n=8 subjects; ICC is presented as estimate [lower bound; upper bound] of 95% confidence interval.